Cancer Science: Open Access

Scient Open Access
Exploring the World of Science

Open Access Full Text Article

Research Article

A Novel Approach for Histopathological Inspection of Surgically Excised Oral Mucosal Lesions: Topographical Mapping of Premalignant Epithelium

This article was published in the following Scient Open Access Journal:
Cancer Science: Open Access
Received November 07, 2016; **Accepted** December 20, 2016; **Published** December 27, 2016

Takuo Henmi[1], Hisao Yagishita[2], Kaori Sato[1], Yuji Taya[1] and Yuuichi Soeno[1*]

[1]Department of Pathology, School of Life Dentistry at Tokyo, The Nippon Dental University, 1-9-20 Fujimi, Chiyoda-ku, Tokyo, 102-8159 Japan
[2]Division of Oral Diagnosis, Dental and Maxillofacial Radiology and Oral Pathology Diagnostic Services, The Nippon Dental University Hospital, 2-3-16 Fujimi, Chiyoda-ku, Tokyo 102-8158, Japan

Abstract

Objective: Cancer-suspected oral mucosa more or less comprise the precancerous field of the epithelium. Here, we aimed to develop a novel system that summarizes histological and immunohistochemical properties of the whole epithelial field of surgically excised specimens.

Methods: Specimens of tongue mucosal lesions were dissected into 3-mm pieces and thin sectioned. Each neighboring section was stained with hematoxylin-eosin (HE) or immunohistochemistry (IHC) for Ki67 and CK13. The epithelial property was evaluated in every 500-μm width (analyzing unit) in each section. A unit with normal or atypical phenotype was coded as "0" or "1", respectively, and compiled in a database. The dataset was then arranged as a topographical map according to the original positional relation to the specimen. For IHC-based maps, both Ki67 and CK13 phenotypes were combined and classified using four color grades, namely, white unit (IHC-intact) and yellow/orange/red units (IHC-atypical).

Results: In total, 25 specimens (5,258 analyzing units) were analyzed. Statistical evaluation confirmed that the combination of Ki67/CK13 phenotypes had outstanding performance to discriminate HE atypism. Topographical mapping demonstrated heterogeneous composition of atypical epithelium, which is rarely disclosed in routine pathological services. The color-grading depicted monocentric or multicentric localization of advanced atypical region, implying distinct expanding modes and modality of atypism among specimens. Comparative map analysis also represented intrinsic discrepancies between HE and Ki67/CK13 atypical statuses in some specimens.

Conclusion: Our original system with region-based inspection and topographical mapping using routine HE/IHC is a fruitful technique to readily comprehend the premalignant property of excised oral mucosal lesions.

Keywords: Oral squamous cell carcinoma, Field cancerization, Tongue, Immunohistochemistry

Introduction

Oral cancers, which are mostly squamous cell carcinomas (SCC), arise from the oral mucosa as a result of diffused and repeated carcinogenic assault, which has been attributed to "field cancerization" [1-3]. In fact, atypical epithelium is often present in the surrounding regions of oral cancer and carries a high risk for local recurrence and emergence of multiple lesions [4-9]. Such an epithelium, however, represents no obvious changes on its surface, particularly in the early phase of the lesion, and is therefore referred to as premalignant epithelium.

In clinical practice, vital iodine staining is utilized to discriminate dysplastic/cancerous epithelium from normal epithelium [5,8,10], and thus we routinely combined with excisional biopsy of oral mucosal lesions. To assist the pathological assessment of excised specimens immunohistochemistry (IHC) has also been used in combination with traditional hematoxylin-eosin (HE) staining. For example, Ki67 overexpression is utilized to evaluate elevation of cell proliferating activity [11,12]. A variety of cytokeratin subtypes are also applied to assess alteration of epithelial phenotypes; loss of cytokeratin 13 (CK13) expression and gain of CK17 expression is one of the features widely exploited to discriminate atypical epithelium from normal epithelium [13-17].

***Corresponding Author:** Yuuichi Soeno, Department of Pathology, School of Life Dentistry at Tokyo, The Nippon Dental University, 1-9-20 Fujimi, Chiyoda-ku, Tokyo 102-8159, Japan, Tel: +81-3-3261-8899, Fax: +81-3-3261-8969, E-mail: soeno-path@tky.ndu.ac.jp

Despite the clinicopathological trend, such molecular evidence has not been used to corroborate the comprehensive picture of field cancerization in the excised specimen, the patient's mucosa. This is partially because routine pathological services concentrate on definitive findings for diagnosis; information about the rest of the region in the specimen is not fully recorded unless remarkable findings exist. Currently, pathologists can yield stable immunohistochemical outcomes by using automated IHC platforms, which are also free of laborious handling steps [18]. Moreover, development of high-resolution image scanners and sophisticated image analysis software makes histopathology more suitable for analytical purposes [19,20]. In the context of such technical advances, we considered that both HE and IHC-based epithelial profiles should be analyzed and compiled in a more systematic manner.

In this study, we aimed to develop a novel system to evaluate histopathological and immunohistochemical properties of the epithelium in the whole region of excised tongue specimens. We examined widthwise localization of HE histology and IHC phenotypes (Ki67, CK13, and CK17), evaluated relationships among these markers, and visualized the competitive landscape of premalignant epithelial populations by means of topographical mapping.

Materials and Methods

Case recruitment

Human tissues were obtained from the Department of Oral and Maxillofacial Surgery, Nippon Dental University Hospital. The use of these archival tissues was in accordance with the provisions of the Declaration of Helsinki for research involving human tissue and was approved by both the Ethics Committee and the Institutional Review Boards of Nippon Dental University. Tongue specimens used in this study were surgically excised according to iodine stainability (5% iodine solution) and pathologically diagnosed as dysplasia or early SCC in routine operation based on the standard histological criteria from the Japanese Societies of Oral Oncology and Oral Pathology [21,22]. In this report, we indicated the diagnosis as oral epithelial dysplasia (OED) or oral cancer (OC) including oral intraepithelial neoplasia and SCC, which represented the very early phase of subepithelial invasion.

Preparation of histological sections and immunohistochemistry

Each formalin-fixed specimen was dissected into 3-mm slices perpendicular to the anterior–posterior axis and embedded in paraffin. Serial 4-μm-thin sections were then mounted onto adhesive glass slides (Platinum Pro; Matsunami Glass, Osaka, Japan). Four neighboring slides were processed for HE staining and IHC. IHC was performed using an automated staining instrument (Ventana Benchmark GX; Ventana Medical System Inc., Oro Valley, AZ, USA) according to the manufacturer's instruction. For detection, a labeled streptavidin-biotin method was used according to the Ventana DAB Universal Kit. Slides were mounted with Entellan New (Merck, Darmstadt, Germany). Mouse monoclonal antibodies (and the working dilution rate) used in this study are as follows: anti-human Ki67 (1:50; MIB-1, Dako Corp., Carpinteria, CA, USA), anti-human CK13 (1:100; DE-K13, Dako), and anti-human CK17 (1:50; E3, Dako).

Histological image digitization and evaluation of epithelial atypism

Images of stained slides were acquired using a 20× objective with a virtual microscope image scanner (NanoZoomer HT, Hamamatsu Photonics, Hamamatsu, Japan). While assessing the appearance of IHC images, we found that stratification of Ki67-positive cells frequently emerged in a narrow window of 300-500 μm. Therefore, we employed 500-μm width as the target subregion size (= analyzing unit). To mark the 500-μm segments, we used virtual slide viewer software (NDP view ver1.2, Hamamatsu Photonics), which retained all marks on the original image.

The epithelial property was evaluated in every analyzing unit; a unit with normal phenotype was coded as "0", and a unit with any remarkable findings was coded as "1" (Figure 1 and Supplementary Figure S1A). Ki67-positive nuclei were normally scattered in the parabasal layer of the epithelium. A unit with this condition was coded as "0". In other cases, Ki67-positive nuclei presented as enlarged and emerged at the basal layer and/or stratified through the epithelial layer. All these aberrant patterns of Ki67 expression were assigned as atypical status and a unit with this condition was coded as "1". CK13 was expressed in all layers of epithelial cells except for the basal layer in normal tongue mucosa. In pathological condition, CK13 expression status varied from partial diminishment to complete loss. Therefore, by definition, intact CK13 expression was coded as "0", while diminished CK13 expression to any degree was coded as "1". In parallel with IHC assessment, HE histology was evaluated by an experienced pathologist (H.Y.) to mark any aberration in epithelial morphology [23]. A unit with normal epithelium was designated as HE-intact and coded as "0", while a unit with any atypical change was designated as HE-atypical and coded as "1".

The defined units were compiled in a database using Microsoft Excel 2013 (Microsoft, Redmond, WA, USA). Each code from individual analyses (Ki67, CK13, and HE) was input into the same row in the datasheet (e.g., 0, 0, 1) to indicate those codes came from the same position in the specimen.

During the evaluation of CK17 expression, we found that faint CK17 expression was often present throughout the epithelium where CK13 expression was intact. This finding was clearly demonstrated by digitized assessment using ImageJ software (NIH, Bethesda, MD, USA) (Supplementary Figure S1B). Because we aimed to evaluate the premalignant status of the oral mucosa as simply as possible, we excluded further examination of CK17 and focused on the assessment of Ki67 and CK13, both of which could be readily judged by visual inspection.

It should be noted that in this report we used the terms "atypical" and "atypism" for any phenotypic changes of epithelium, which has implications on potential malignancy.

Topographical mapping and statistical evaluation

Upon case selection, we checked for units in which the condition was indeterminate owing to epithelial failure, such as presence of an ulcer, thereby using cases in which over 75% of units were available for analysis. Finally, we analyzed 25 specimens in this study. The defined units were arranged in an original sequence of dissected slices on the Excel database and superimposed onto the

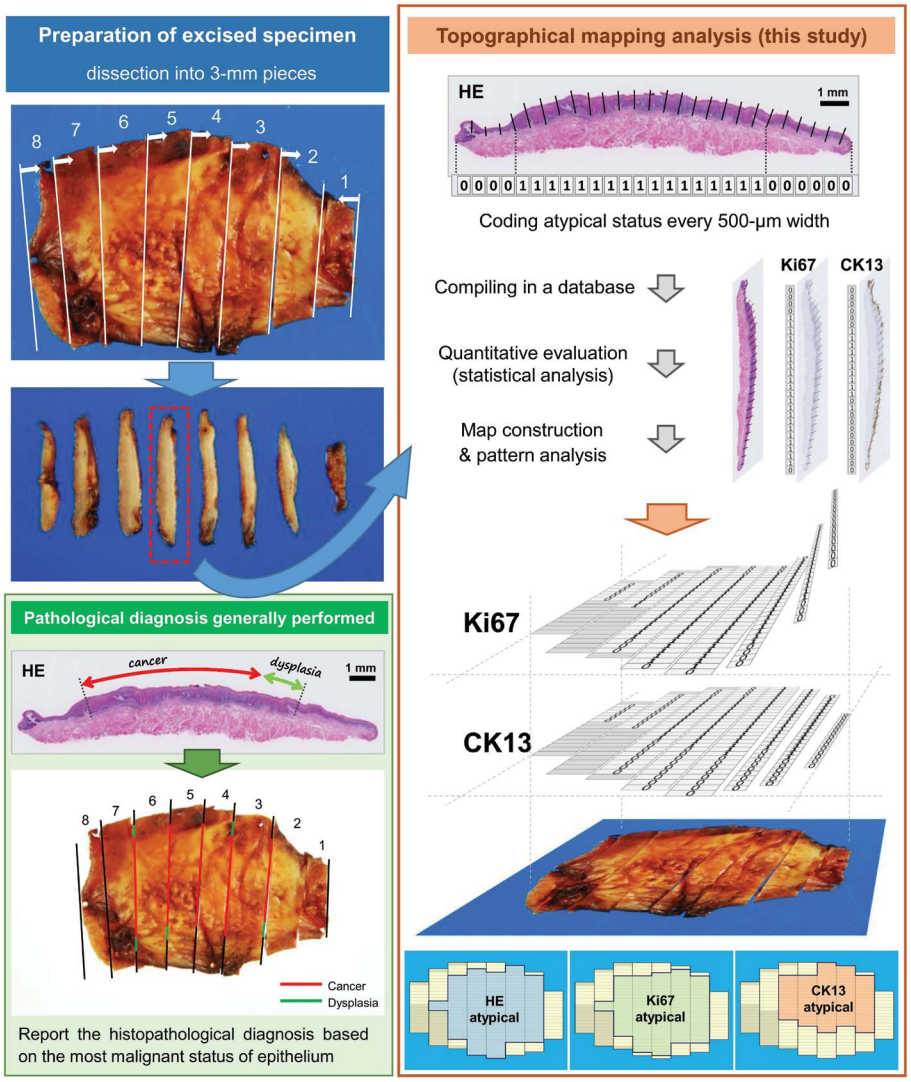

Figure 1. Pathological evaluation of specimens both in general and in this study. A formalin-fixed mucosal specimen is further dissected into 3-mm pieces, paraffin-embedded, and thin sectioned. In pathological services, each specimen is evaluated by histological appearance and finally diagnosed. Details about the epithelial status may be reported if specific findings localize somewhere in the specimen (green box). In this study, the malignant status of the epithelium (atypism) is evaluated every 500 μm and converted into a binary code: "0" for normal and "1" for atypical (orange box). We adopt this procedure for HE staining and IHC for Ki67 and CK13. Compiled data are then statistically analyzed. Based on the coded information, we construct topological maps to evaluate visually the malignant status of the epithelium throughout the entire specimen.

corresponding macroscopic image so that the distribution of atypical phenotypes was rebuilt on the map (Figure 1).

Descriptive statistics including cross tabulation were performed using SPSS statistics software version 24 (IBM Japan, Tokyo, Japan). Univariate and multivariable logistic regression analyses were also performed to estimate associations between immunohistochemical profiles and morphological (HE-based) findings. Receiver operating characteristic (ROC) analysis was also used to determine the diagnostic value of atypical epithelial condition. A value of $P < 0.05$ was considered statistically significant.

Results

Statistics of field properties

In all marked units from the 25 specimens (n=5,258), 49.4% of all units (2,599/5,258) were judged as Ki67-atypical, while 35.3% (1,855/5,258) were CK13-atypical. Involvement of IHC phenotype in HE-atypical status was also evaluated using univariate logistic regression analysis. Ki67- and CK13-atypical conditions were significantly associated with HE-atypical status compared with normal condition of each marker ($P < 0.001$) (Table 1). The significance of Ki67 and CK13 was also confirmed by a multivariate model, which had a satisfactory goodness of fit (Hosmer–Lemeshow test; $\chi^2 = 1.88$, $P = 0.39$). Notably, when Ki67-atypical status coincided with CK13-atypical status, such condition was more relevant to HE-atypical status with a high odds ratio (odds ratio 33.5, 95% CI 27.3-41.0). To evaluate the ability to detect HE atypism, ROC curve analysis was applied to each marker. The area under the curve (the more value, the better discriminative ability) for Ki67 and CK13 were 0.75 and 0.74, respectively (cutoff value = 0.5), while that of Ki67/CK13 combination was 0.81.

Parameter			OR	95%CI	p-value
Ki67			9.1	8.1 - 10.4	< 0.001*
CK13			13.5	11.6 - 15.8	< 0.001*
Ki67	CK13				
0	0	(white)	1	-	
0	1	(yellow)	6	4.6 - 7.8	< 0.001*
1	0	(orange)	4.4	3.8 - 5.1	< 0.001*
1	1	(red)	33.5	27.3 - 41.0	< 0.001*

OR, odds ratio; CI, confidence interval; * $P < 0.05$.

Table 1. Logistic regression analysis for predicting HE-atypism

Topographical mapping of IHC/HE-based atypism

The data of atypical epithelial status were then arranged as a topographical map. In this process, a set of coding data were aligned according to the original positional relation by which the specimen shape was reconstructed (Figure 1). In response to the statistical finding, we conducted combinatorial representation for Ki67 and CK13 phenotypes. Namely, we arranged the Ki67 and CK13 expression status into four color grades according to the criteria detailed in Figure 2: Ki67/CK13 0/0 as (warm-)white unit, 0/1 as yellow unit, 1/0 as orange unit, and 1/1 as red unit.

Resulting maps from all 25 specimens were sorted in descending order of the %IHC-atypical area, i.e., the coverage of the IHC-atypical region (the sum of yellow, orange, and red units) within the specimen (Figure 3A). The %IHC-atypical area varied from 100.0% at maximum to 13.6% at minimum, with a mean of 56.7% ± 26.1% (Table 2). In an overview of IHC maps, cases #1-13 were rich in "atypical" color units, i.e., few white units. In these specimens, red and orange units occupied most of the

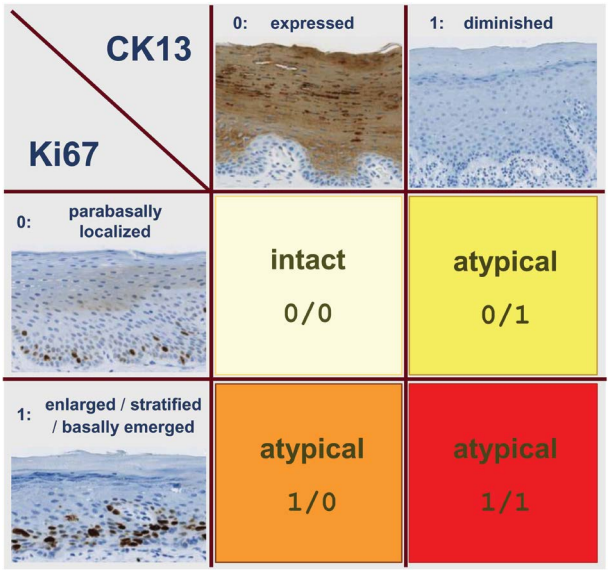

Figure 2. Color grading of IHC-based atypism. Color-coded classification of the epithelial condition based on the Ki67 and CK13 expression patterns.

Case ID	Size of specimen (number of units)	IHC-atypical area (%)	HE-atypical area (%)	IHC-positivity at the margin			Final Diagnosis
				yellow	orange	red	
#1	70	100	71	-	+	+	OED
#2	152	96.5	44.7	-	+	-	OC
#3	113	95.2	86.5	-	+	+	OC
#4	85	94.3	100	-	+	+	OED
#5	285	88.1	72.7	-	+	+	OC
#6	342	81.5	78.4	+	+	+	OC
#7	194	70.6	71.8	+	-	-	OC
#8	310	69.9	55.6	-	+	+	OC
#9	243	69.7	56.4	-	+	-	OED
#10	622	64.6	45.4	+	-	-	OC
#11	295	63.6	70.6	-	+	-	OC
#12	291	62.3	41.2	+	+	-	OC
#13	371	54.7	52	-	+	+	OC
#14	165	53.4	86.5	-	-	-	OED
#15	223	52.5	84.9	+	+	+	OED
#16	290	45.6	42.6	-	+	-	OC
#17	106	44	54.7	-	+	-	OED
#18	270	39	48.3	-	+	-	OED
#19	280	33.2	40.2	-	-	-	OC
#20	256	32.9	39.1	-	-	-	OC
#21	479	28.5	18.4	-	-	-	OC
#22	243	23.9	51.2	-	+	-	OED
#23	217	21.8	36.4	-	-	-	OC
#24	90	15.5	46.4	+	+	-	OED
#25	80	13.6	87.9	-	+	-	OED

The 25 cases analyzed and numbered according to the ratio of the IHC-atypical region are shown in descending order. Presence of IHC-atypical region at the surgical margin is indicated as either positive (+) or negative (-). Final pathological diagnosis for each specimen is also shown. OC, oral cancer (including oral intraepithelial neoplasia and SCC); OED, oral epithelial dysplasia.

Table 2. Excised tongue specimens analyzed in this study

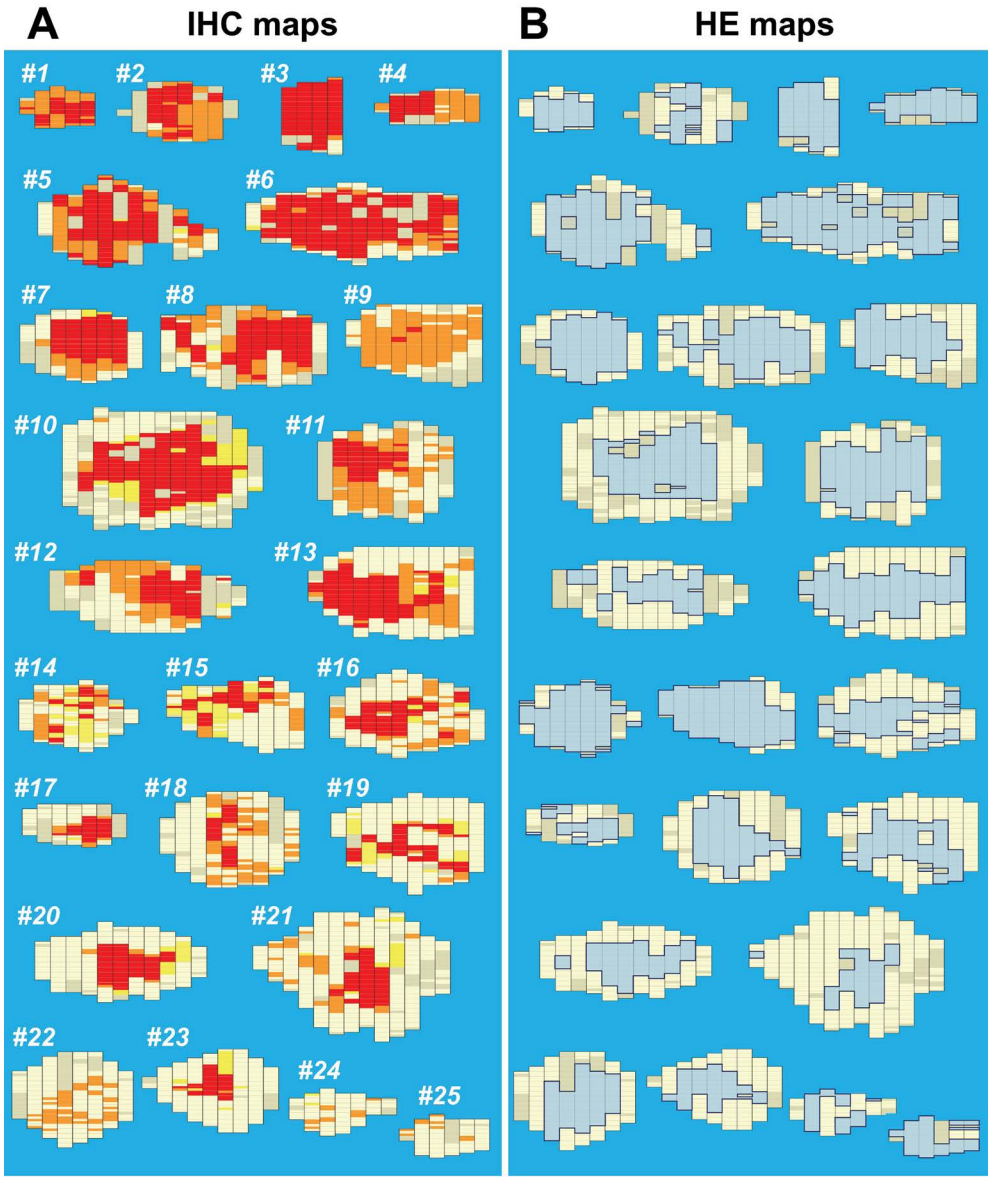

Figure 3. Representation of topographical mapping for 25 tongue specimens. (A) IHC-based mapping of epithelial atypism. Color grading is based on the criteria in Figure 2. Specimens are arranged in descending order according to the coverage of atypical units within the specimen. (B) Corresponding HE-based maps. Histologically atypical regions are depicted as light blue panels. Each case number shown in IHC maps corresponds to the respective ID number in Table 2.

region including the outer margin of the specimen (particularly specimens #1-4; %IHC-atypical area, >90%). On closer inspection, red units typically formed a mass that localized to the central portion of the specimen or appeared as multiple loci. Orange units had a propensity to localize around the red area. In contrast, white-dominated specimens, i.e., cases #14-25, represented diverse color distribution such as a locally-restricted red area (#17, #20, and #23), narrow expansion of red/orange units (#15 and #19), and scattered orange areas (#18, #21, and #22). When examined the margins of these IHC-maps, 20 out of 25 cases (80.0%) possessed marginal exposure of IHC-atypical region (Table 2).

In contrast, corresponding HE maps showed that the HE-atypical area was mostly present in the central portion of the specimen (Figure 3B). The coverage of the HE-atypical region within each specimen (%HE-atypical area) varied from 100% to 18.4%, with a mean of 59.3% ± 20.0% (Table 2). The correlation between the %IHC-atypical area and %HE-atypical area was moderate (r=0.464). In this regard, discrepancy between IHC-atypical and HE-atypical occupancies were noticeable in some cases. Notably, cases #14 and #15 had %IHC-atypical area of 53.4% and 52.5%, respectively, while their %HE-atypical area represented 86.5% and 84.9%, respectively (Figure 3 and Table 2).

Discussion

We herein established a system that facilitates analyzing the epithelial condition throughout the entire region of excised tongue specimens. Together with many technical advantages, we achieved a better understanding of the premalignant epithelial field as described below.

Evaluation of field composition and molecular markers

In general, pathological specimens are sliced in 3-mm sections. In human skin, the size of the clonal population (patch) of keratinocytes is approximately 2 mm in diameter [24]. In this context, observation at every 2- to 3-mm width would satisfy screening purposes. In this study, we employed a 500-μm analyzing unit. Although analysis with this resolution was restricted to the dorsal-ventral axis of the specimen, it provided a clearer landscape of the epithelial field. Moreover, this region-based analysis helped to statistically assess the potential application of molecular markers. We confirmed that the combination of Ki67/CK13 phenotypes provides outstanding performance to discriminate HE atypism. This concept has been pointed out by Yagyuu et al., who assessed diagnostic/prognostic IHC values using low-grade and high-grade dysplasia cases [17]. Importantly, we reached almost the same conclusion as a result of whole-region specimen assessment; this study analyzed 5,258 segments from 25 specimens. We put emphasis that this system has a great versatility to cumulative cases and molecular markers and is much applicable to take marker-to-marker relevance into account toward a holistic interpretation of the premalignant field of the oral epithelium.

Premalignant epithelial properties of excised specimens

Using topographical mapping, we demonstrated heterogeneous composition of atypical epithelium, which is rarely disclosed in routine pathological services. Of 25 map pairs, a majority of specimens contained a certain amount of both red and orange units; typically representing a red-unit mass at the center (monocentric), while a couple of specimens exhibited intermittently localized red-unit populations (multicentric) surrounded by orange units. This is in line with previous findings that the region suspected to be precancerous exhibited active proliferation and the patchy field of precancerous epithelium clonally expanded to the tissue [4,25-27]. However, we found orange foci that were not gathered but scattered in the specimen (e.g., #18, #21, and #22). This might reflect reactive change of the epithelium; namely, such regions are not yet committed to malignant transition. We also encountered another pattern that exhibited narrow expansion of red units with tortuous appearance (e.g., #15 and #19). In such cases, red units were adjoined by yellow units rather than orange units, implying that atypism proceeded with local diminishment of CK13 expression. Because the incidence of yellow units was less frequent than other atypical units, a diminished CK13 expression status might be transient and promptly shift to proliferative (changes to red).

Overall, color-graded mapping of Ki67/CK13 phenotypes provided a great advantage to presume the modality of atypism. The results may reflect different expanding phases owing to the timing of surgical excision of individual cases. These spatial and temporal perspectives are important for comparing primary/recurrent lesion pairs as well as multiple primary lesions.

Extrapolating the whole epithelial field of the patient's mucosa

Topographical information of atypical epithelium also provides clues about the oral mucosa status, which was once contiguous with each specimen. A specimen filled with "atypical" color units likely indicates increased potency of malignant epithelium in the patient. For instance, cases #1 and #4, although diagnosed as OED (i.e., dysplasia), should be closely followed up.

In this context, patients who provided white-dominated specimens may have oral mucosa with less cancerous risk. Cases #20, #21, and #23 were diagnosed as cancer; however, their IHC maps represented a restricted malignant portion that was surrounded by white IHC-intact regions including excisional margins. The corresponding HE maps depicted the same condition. In contrast, OED cases #14 and #15 had a considerably higher HE-atypical occupancy than IHC-atypical occupancy (Figure 3 and Table 2). Thus, interpretation of white-dominated cases may be challenging; such cases must be closely monitored using occult phenotypic changes other than Ki67/CK13 phenotypes. Potential candidate markers that should be further studied include CK17 and p53 [28,29]. We believe that progressive accumulation of assessments of marker-to-marker relevance will result in identification of a better combination of markers that will achieve more accurate pathological diagnosis.

Additionally, information about the extent of atypical epithelium, including the status at the excisional margin (in this study 80% of samples had atypical IHC status at their margins) helps clinicians with treatment planning. We have already found that the visual report we provide facilitates discussion with clinicians; significantly improving the understanding of pathologists and clinicians of the pathological condition of patients' mucosa. Appropriate surgical management improves diagnostic accuracy.

Conclusion and Outlook

We conclude that premalignancy of the epithelium should be defined not only by molecular marker positivity but also by distribution patterns within the specimen, which can be achieved only by using a mapping approach. A recent report noted that histological examination of whole excised tissue appears to be essential and that there is a need to develop hands-on methods for the identification of oral mucosa at risk for future cancer development [30]. In this regard, an advantage of our mapping approach is that it does not require any specific device or reagent. However, even our latest protocol takes several hours per specimen to evaluate IHC phenotypes and subsequently integrate data. We acknowledge that further improvements in rapid collection and gathering of data are required, for instance, by development of a computer-assisted image analyzing system.

Acknowledgments

This work was supported by a grant-in-aid from the Japanese Ministry of Education, Culture, Sports, Science and Technology (KAKENHI 25463154).

Conflict of Interest

The authors declare no potential conflicts of interest with respect to the authorship and/or publication of this article.

References

1. Slaughter DP, Southwick HW, Smejkal W. Field cancerization in oral stratified squamous epithelium; clinical implications of multicentric origin. *Cancer.* 1953;6(5):963-968.

2. Leemans CR, Braakhuis BJM, Brakenhoff RH. The molecular biology of head and neck cancer. *Nat Rev Cancer.* 2011;11(1):9-22.

3. Angadi PV, Savitha JK, Rao SS, Sivaranjini Y. Oral field cancerization: current evidence and future perspectives. *Oral Maxillofac Surg.* 2012;16(2):171-180.
4. van Houten VMM, Tabor MP, van den Brekel MWM, et al. Mutated p53 as a molecular marker for the diagnosis of head and neck cancer. *J Pathol.* 2002;198(4):476-486.
5. Gorsky M, Epstein JB, Oakley C, Le ND, Hay J, Stevenson-Moore P. Carcinoma of the tongue: A case series analysis of clinical presentation, risk factors, staging, and outcome. *Oral Surg Oral Med Oral Pathol Oral Radiol Endod.* 2004;98(5):546-552.
6. Tabor MP, Brakenhoff RH, Ruijter-Schippers HJ, Kummer JA, Leemans CR, Braakhuis BJ. Braakhuis BJ. Genetically altered fields as origin of locally recurrent head and neck cancer: a retrospective study. *Clin Cancer Res.* 2004;10(11):3607-3613.
7. Schaaij-Visser TB, Graveland AP, Gauci S, et al. Differential proteomics identifies protein biomarkers that predict local relapse of head and neck squamous cell carcinomas. *Clin Cancer Res.* 2009;15(24):7666-7675.
8. Ganly I, Patel S, Shah J. Early stage squamous cell cancer of the oral tongue-Clinicopathologic features affecting outcome. *Cancer.* 2012;118(1):101-111.
9. Simple M, Suresh A, Das D, Kuriakose MA. Cancer stem cells and field cancerization of Oral squamous cell carcinoma. *Oral Oncol.* 2015;51(7):643-651.
10. Maeda K, Suzuki T, Ooyama Y, et al. Colorimetric analysis of unstained lesions surrounding oral squamous cell carcinomas and oral potentially malignant disorders using iodine. *Int J Oral Maxillofac Surg.* 2010;39(5):486-492.
11. Takeda T, Sugihara K, Hirayama Y, Hirano M, Tanuma JI, Semba I. Immunohistological evaluation of Ki-67, p63, CK19 and p53 expression in oral epithelial dysplasias. *J Oral Pathol Med.* 2006;35(6):369-375.
12. Gonzalez-Moles MA, Bravo M, Ruiz-Avila I, et al. Ki-67 expression in non-tumour epithelium adjacent to oral cancer as risk marker for multiple oral tumours. *Oral Dis.* 2010;16(1): 68-75.
13. Ohta K, Ogawa I, Ono S, et al. Histopathological evaluation including cytokeratin 13 and Ki-67 in the border between Lugol-stained and -unstained areas. *Oncol Rep.* 2010;24(1):9-14.
14. Mikami T, Cheng J, Maruyama S, et al. Emergence of keratin 17 vs. loss of keratin 13: Their reciprocal immunohistochemical profiles in oral carcinoma in situ. *Oral Oncol.* 2011;47(6): 497-503.
15. Sakamoto K, Aragaki T, Morita K, et al. Down-regulation of keratin 4 and keratin 13 expression in oral squamous cell carcinoma and epithelial dysplasia: A clue for histopathogenesis. *Histopathology.* 2011;58(4):531-542.
16. Nobusawa A, Sano T, Negishi A, Yokoo S, Oyama T. Immunohistochemical staining patterns of cytokeratins 13, 14, and 17 in oral epithelial dysplasia including orthokeratotic dysplasia. *Pathol Int.* 2014;64(1):20-27.
17. Yagyuu T, Obayashi C, Ueyama Y, et al. Multivariate analyses of Ki-67, cytokeratin 13 and cytokeratin 17 in diagnosis and prognosis of oral precancerous lesions. *J Oral Pathol Med.* 2015;44(7):523-531.
18. Prichard JW. Overview of automated immunohistochemistry. *Arch Pathol Lab Med.* 2014;138(12):1578-1582.
19. Hamilton PW, Bankhead P, Wang Y, Hutchinson R, Kieran D, et al. Digital pathology and image analysis in tissue biomarker research. *Methods.* 2014;70(1):59-73.
20. Saeed-Vafa D, Magliocco AM. Practical applications of digital pathology. *Cancer Control.* 2015;22(2):137-141.
21. Japan Society for Oral Tumors. General Rules for Clinical and Pathological Studies on Oral Cancer. 1st edn. Tokyo: Kanehara & Co. Ltd. 2010 (in Japanese).
22. Saku T, et al. Carcinoma in-situ of the oral mucosa: Its pathological diagnostic concept based on the recognition of histological varieties proposed in the JSOP oral CIS catalog. *J Oral Maxillofac Surg Med Pathol.* 2014;26:397-406.
23. Gale N, Pilch BZ, Sidransky D, El Naggar A, Westra W, et al. (2005) Epithelial precursor lesions. In: Barnes L, Everson JW, Reichart P, Sindransky D, eds. World Health Organization classification of tumors: pathology and genetics of head and neck tumours. Lyon: IARC, 177-179, 140-143.
24. Chaturvedi V, Chu MDS, Carrol BSM, Brenner BSJW, Nickoloff BJ. Estimation of size of clonal unit for keratinocytes in normal human skin. *Arch Pathol Lab Med.* 2002;126(4):420-424.
25. van Oijen MG, Gilsing MM, Rijksen G, Hordijk GJ, Slootweg PJ. Increased number of proliferating cells in oral epithelium from smokers and ex-smokers. *Oral Oncol.* 1998;34(4): 297-303.
26. Tang XH, Scognamiglio T, Gudas LJ. Basal stem cells contribute to squamous cell carcinomas in the oral cavity. *Carcinogenesis.* 2013;34(5):1158-1164.
27. Alcolea MP, Greulich P, Wabik A, Frede J, Simons BD, Jones PH. Differentiation imbalance in single oesophageal progenitor cells causes clonal immortalization and field change. *Nat Cell Biol.* 2014;16(6):615-622.
28. Cruz I, Napier SS, Van der Waal I, et al. Suprabasal p53 immunoexpression is strongly associated with high grade dysplasia and risk for malignant transformation in potentially malignant oral lesions from Northern Ireland. *J Clin Pathol.* 2002;55(2):98-104.
29. Van der Vorst S, Dekairelle AF, Weynand B, Hamoir M, Gala JL. Assessment of p53 functional activity in tumor cells and histologically normal mucosa from patients with head and neck squamous cell carcinoma. *Head Neck.* 2012;34(11):1542-1550.
30. Holmstrup P, Dabelsteen E. Oral leukoplakia-to treat or not to treat. *Oral Dis.* 2016;22(6): 494-497.